

# Coexistence of pairing gaps in three-component Fermi gases

**O.H.T. Nummi, J.J. Kinnunen and P. Törmä**

Department of Applied Physics, P.O. Box 5100, 02015 Aalto University, Finland

E-mail: paivi.torma@hut.fi

**Abstract.** We study a three-component superfluid Fermi gas in a spherically symmetric harmonic trap using the Bogoliubov-deGennes method. We predict a coexistence phase in which two pairing field order parameters are simultaneously nonzero, in stark contrast to studies performed for trapped gases using local density approximation. We also discuss the role of atom number conservation in the context of a homogeneous system.

Submitted to: *New J. Phys.*

## 1. Introduction

Multicomponent ultracold Fermi gases allow the study of several interesting questions in many-body quantum physics. In particular, understanding three-component pairing can reveal some properties of multi- or two-component pairing. In three-component systems the pairing energy does not only compete with temperature effects or Fermi surface mismatch energy but also with other pairing gaps. As in imbalanced two-component systems, non-BCS pairing mechanisms such as Larkin-Ovchinnikov-Fulde-Ferrel (LOFF) [1, 2], breached pairing (BP) [3] and phase separation phases are expected.

Ultracold Fermi gases have opened up a way to explore multi-component gases experimentally. Recently, a degenerate three-component gas was successfully created [4, 5]. The stability of three-component gases is hindered by the three-body recombination, reducing the pairing in the gas and the lifetime of the sample [6, 7, 8]. However, there are ways to stabilize the gas against such losses using for example optical lattices. Optical lattices are interesting also due to the rich phase diagram: theoretical investigations have found that color superconductivity competes with normal phase and formation of trions [9, 10, 11, 12, 13, 14, 15].

Both the  $SU(3)$  symmetric model, in which the different components have identical properties, and the non- $SU(3)$  symmetric case have been widely studied [16, 17, 18, 19, 20, 21, 22, 23, 24, 25]. The particularly important special case of  $SU(3)$  symmetry can be realized using alkaline earth atoms [26] or in optical lattices. However, with alkaline earth atoms the numbers of atoms in different components are not well defined, and only the total number of atoms is conserved. In contrast, the hyperfine energy spacing in alkaline atoms stabilizes the atom numbers, making the atom number of each component separately conserved. This is the case of most two-component Fermi gas experiments and a natural extension of these studies is a non- $SU(3)$  symmetric case in which the atom numbers in all three components are fixed.

Here we study such a three-component system with fixed atom numbers in all three components in a spherically symmetric harmonic trap using the Bogoliubov-deGennes (BdG) equations. We study the coexistence of the pairing gaps in these systems and discuss the scaling of the system size up to the thermodynamical limit.

In section 2 we give an overview of the three-component system and the corresponding mean-field theory. In the next section 3 we consider the BCS-type mean-field theory in homogeneous space and describe the effect of boundary conditions on the stability of different phases. In section 4 we consider the effects of trapping potential using the BdG method. In section 5 we show the main results obtained from the BdG method, especially regarding the coexistence of two pairing gaps. We conclude by discussion in section 6.

## 2. The system setup

The general mean-field Hamiltonian for a three-component system in the contact interaction potential approximation is (up to a constant)

$$H_{\text{MF}} = \sum_{\sigma=1,2,3} \int d^3r \Psi_{\sigma}^{\dagger}(\mathbf{r}) \left[ -\frac{\hbar^2 \nabla^2}{2m_{\sigma}} + V_{\sigma}(\mathbf{r}) - \mu_{\sigma} + W_{\sigma}(\mathbf{r}) \right] \Psi_{\sigma}(\mathbf{r}) \quad (1)$$

$$+ \frac{1}{2} \sum_{\sigma \neq \sigma'} \int d^3r \Delta_{\sigma\sigma'}(\mathbf{r}) \Psi_{\sigma}^{\dagger}(\mathbf{r}) \Psi_{\sigma'}^{\dagger}(\mathbf{r}) + h.c., \quad (2)$$

where the first term of the Hamiltonian includes contributions from the kinetic energy, the external trapping potential  $V_{\sigma}(\mathbf{r})$  (that can depend on the component  $|\sigma\rangle$ ), and the chemical potentials  $\mu_{\sigma}$ , respectively. Interactions are described by the two-body scattering T-matrix. In the contact interaction potential approximation it can be written as

$$U_{\sigma\sigma'}(\mathbf{r}, \mathbf{r}') = \frac{4\pi\hbar^2 a_{\sigma\sigma'}}{m_r} \delta(\mathbf{r} - \mathbf{r}'), \quad (3)$$

where  $a_{\sigma\sigma'}$  is the scattering length between atoms in hyperfine states  $|\sigma\rangle$  and  $|\sigma'\rangle$ , and  $m_r = 2m_{\sigma}m_{\sigma'}/(m_{\sigma} + m_{\sigma'})$  is twice the reduced mass. The Hartree fields are denoted by  $W_{\sigma}(\mathbf{r}) = \sum_{\sigma \neq \sigma'} U_{\sigma\sigma'}(\mathbf{r}) n_{\sigma'}(\mathbf{r})$  and the densities are  $n_{\sigma}(\mathbf{r}) = \langle \Psi_{\sigma}^{\dagger}(\mathbf{r}) \Psi_{\sigma}(\mathbf{r}) \rangle$ . The pairing (mean-)field  $\Delta_{\sigma\sigma'}(\mathbf{r}) = \tilde{U}_{\sigma\sigma'}(\mathbf{r}) \langle \Psi_{\sigma}(\mathbf{r}) \Psi_{\sigma'}(\mathbf{r}) \rangle$  includes a renormalized interaction  $\tilde{U}_{\sigma\sigma'}(\mathbf{r})$  that is used to remove the ultraviolet divergence following the standard procedure (see below). In our model we neglect the possibility of three-body bound states and other three-body effects that can affect the lifetime of the gas [7].

A three-component system has three possible pairing fields corresponding to the three interaction channels  $U_{12}$ ,  $U_{13}$ ,  $U_{23}$ , and these can be combined into a total pairing field vector  $\mathbf{\Delta} = [\Delta_{23}, -\Delta_{13}, \Delta_{12}]^T$ . Identical properties make the system SU(3)-symmetric and the pairing vector can be reduced to a single gap by a simple unitary transformation. The orientation of the pairing vector corresponds to a choice of the global gauge [16, 17, 18, 19, 25], and the simplest choice is the one where only one of the pairing gaps, say  $\Delta_{12}$ , is nonzero. This of course makes atoms in component  $|3\rangle$  effectively noninteracting. Indeed, in an SU(3)-symmetric case, there always exists a gapless branch describing unpaired atoms.

In our study one interaction is always suppressed (we choose  $U_{13} = 0$ ). This is the case for example in  ${}^6\text{Li}$  where Feshbach resonances between the three lowest hyperfine states  $|1\rangle - |2\rangle$  (at  $B = 834$  G) and  $|2\rangle - |3\rangle$  (at  $B = 811$  G) lie close to each other, while the resonance  $|1\rangle - |3\rangle$  (nearest one at  $B = 690$  G) is sufficiently far away [27]. Similar behavior occurs in  ${}^{40}\text{K}$  [28], where the richness of the hyperfine level structure allows even more freedom in choosing the suitable interaction strengths. Moreover, mixtures of  ${}^6\text{Li}$  and  ${}^{40}\text{K}$  offer interesting possibilities [29, 30]. Also we do not consider here interactions between  $|1\rangle$  and  $|3\rangle$  induced by the component  $|2\rangle$  [31]. Thus, neglecting the  $|1\rangle - |3\rangle$  interaction channel altogether, the symmetry is broken at least to SU(2)×SU(1). Analogously to the SU(3) symmetric case, the total pairing field is now a

two-dimensional vector  $\mathbf{\Delta} = [\Delta_{12}, \Delta_{23}]^T$  and in the symmetric case, where components  $|1\rangle$  and  $|3\rangle$  are identical, it is preserved under spin rotations of the hyperfine states  $|1\rangle$  and  $|3\rangle$ . This symmetry implies that the ground state is degenerate with respect to the orientation of the total pairing field vector. However, the degeneracy is lifted by changing masses, chemical potentials or interaction strengths and, as we will soon show, also by imposing boundary conditions such as fixing the number of atoms in different components.

Boundary conditions, such as fixed particle numbers or fixed chemical potentials, manifest themselves in different ways in atomic gases. While the total particle numbers are, in practice, fixed, the local densities are not as the particles are allowed to move around in the trap. Hence, from the local density approximation (LDA) point of view, locally the relevant boundary condition appears to be a fixed chemical potential. However, globally the relevant boundary condition is the fixed particle number, and in the BdG method we indeed fix the mean particle number. Below we will also discuss how the two pictures merge in the limit of large system size  $N \rightarrow \infty$ .

### 3. Homogeneous system

For a homogeneous system the densities and gaps lose their spatial dependence. This corresponds to the usual BCS-approximation in which pairing can only occur between atoms with opposite momenta  $|\mathbf{k}, \sigma\rangle$  and  $|-\mathbf{k}, \sigma'\rangle$ . The mean-field Hamiltonian can be written in matrix form as

$$H_{\text{MF}} = \sum_{\mathbf{k}} \begin{pmatrix} c_{1\mathbf{k}}^\dagger \\ c_{2-\mathbf{k}}^\dagger \\ c_{3\mathbf{k}}^\dagger \end{pmatrix}^T \begin{pmatrix} \xi_{1\mathbf{k}} & \Delta_{12} & 0 \\ \Delta_{12} & -\xi_{2-\mathbf{k}} & \Delta_{23} \\ 0 & \Delta_{23} & \xi_{3\mathbf{k}} \end{pmatrix} \begin{pmatrix} c_{1\mathbf{k}} \\ c_{2-\mathbf{k}}^\dagger \\ c_{3\mathbf{k}} \end{pmatrix} + C, \quad (4)$$

where  $C$  is constant and the single-particle dispersion is  $\xi_{\sigma\mathbf{k}} = \frac{\hbar^2 k^2}{2m_\sigma} - \mu_\sigma$ . We have here neglected the Hartree fields since at the level of our approximation they provide only a constant energy shift in a homogeneous system. The standard approach calls for diagonalizing this using the Bogoliubov transformation, and iteratively solving for the pairing fields  $\Delta_{12}$  and  $\Delta_{23}$ . In order to satisfy the fixed mean atom number boundary condition, the iteration must adjust the chemical potentials in a self-consistent manner as well. Notice that the inherent atom number fluctuations implied by the mean-field theory play no role here as long as the typical fluctuations (scaling as  $\sqrt{N}$ ) are much smaller than the atom numbers in different species (scaling as  $N$ ).

As discussed above, in the symmetric case ( $\mu_1 = \mu_3$ ,  $m_1 = m_3$ ,  $U_{12} = U_{23}$ ), the Hamiltonian has  $\text{SU}(2) \times \text{SU}(1)$  symmetry and all the pairing fields with  $\Delta_{12}^2 + \Delta_{23}^2$  constant yield the same total energy. The ground state is thus degenerate. However, different orientations of the pairing field vector yield different atom numbers in components  $|1\rangle$  and  $|3\rangle$ . Thus, fixing the numbers of atoms  $N_1$  and  $N_3$  breaks the degeneracy and a well-defined energy minimum is found. Figure 1 shows typical energy landscapes  $\langle H_{\text{MF}} + \sum_\sigma \mu_\sigma N_\sigma \rangle$  as a function of the pairing fields  $\Delta_{12}$  and  $\Delta_{23}$  for equal

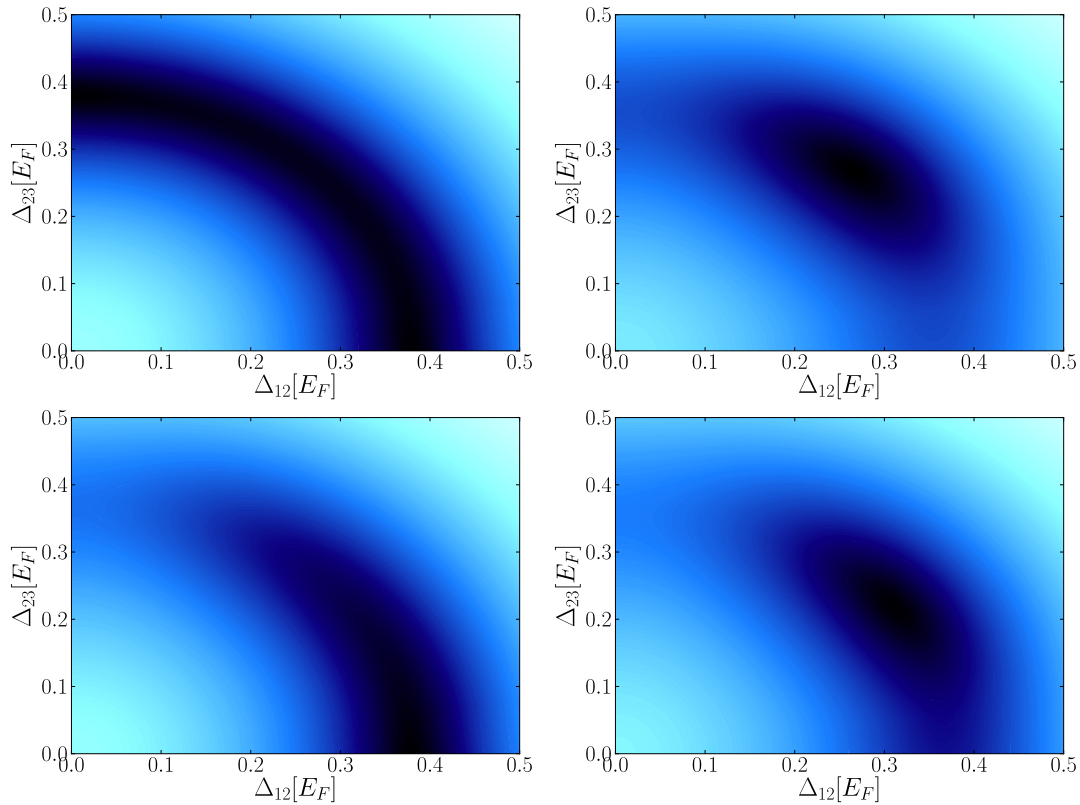


**Figure 1.** Logarithmic energy landscape with constant particle numbers (a)  $N_1 = N_3 = 1.0N_2$  (b)  $N_1 = N_3 = 1.2N_2$  (c)  $N_1 = N_2, N_3 = 1.1N_2$  (d)  $N_1 = 1.1N_2, N_3 = 1.2N_2$ . The interaction strengths are equal  $(k_F a_{12})^{-1} = (k_F a_{23})^{-1} = -0.5$ , ( $k_F = (6\pi^2 n_2)^{1/3}$ ).

interaction strengths  $U_{12} = U_{23}$ . The Fermi momentum  $k_F$  here and throughout this work is defined as the Fermi momentum of the component  $|2\rangle$ ,  $k_F = \sqrt{2mE_F^{\sigma=2}}/\hbar$ , where  $E_F^\sigma$  is the Fermi energy of the component  $|\sigma\rangle$ . The energies have been calculated for fixed atom numbers: the chemical potentials  $\mu_\sigma$  are solved for every point  $(\Delta_{12}, \Delta_{23})$  so that the atom number constraints are satisfied. The figures show clearly how the ground state becomes non-degenerate and realizes itself in a particular combination of pairing fields. In the special case where there is equal number of atoms in all three components,  $N_1 = N_2 = N_3$ , the ground state is still degenerate. However, if the number of atoms in component  $|2\rangle$  is changed (keeping  $N_1 = N_3$  but  $N_2 \neq N_1$ ), the degeneracy is broken and a non-degenerate energy minimum appears. This is in stark contrast to the case where the chemical potentials are kept constant and the atom numbers are allowed to vary. In such a case the ground state remains degenerate as long as the chemical potentials for components  $|1\rangle$  and  $|3\rangle$  are equal,  $\mu_1 = \mu_3$ .

In the case of a number mismatch or difference in the interaction strengths of the components  $|1\rangle$  and  $|3\rangle$ , the energy minimum will be shifted from the equal pairing case. Depending on the number of atoms in component  $|2\rangle$ , the minimum appears either at the edge of the energy landscape (yielding either of the two pairing fields  $\Delta_{12}$  or  $\Delta_{23}$  zero) or

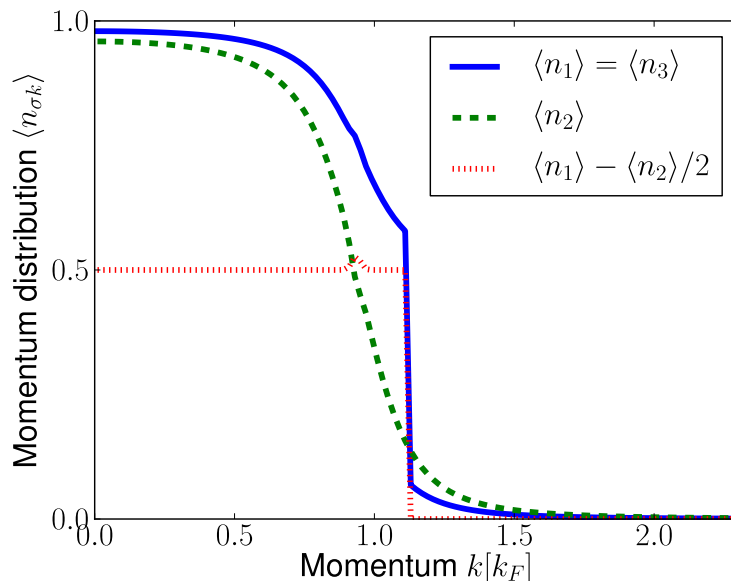


**Figure 2.** The single-particle occupation numbers for  $N_1 = N_3 = 1.2N_2$  and equal pairing fields  $\Delta_{12} = \Delta_{23} = 0.25E_F$ . All atoms in the hyperfine state  $|2\rangle$  are paired but part of the atoms in components  $|1\rangle$  and  $|3\rangle$  are unpaired. The unpaired atoms form a well-defined Fermi sphere resulting in a step at the Fermi surface.

somewhere in between. This too is an important difference to the case of fixed chemical potentials where the breaking of the symmetry (by either changing chemical potentials or interaction strengths) always results in either of the two pairing fields dominating and the other becoming zero. Thus, for fixed chemical potentials one does not observe *coexistence* of the two pairing fields  $\Delta_{12}$  and  $\Delta_{23}$  except possibly in the symmetric, or degenerate, case, whereas for fixed atom numbers the coexistence phase (described by two non-vanishing pairing field order parameters  $\Delta_{12}$  and  $\Delta_{23}$ ) is very real.

The pairing scheme is revealed by the momentum distribution of each state. Figures 2 and 3 show the momentum distributions of the three components for equal pairing gaps ( $\Delta_{12} = \Delta_{23}$ ) and for projected pairing gaps (obtained by setting  $\Delta_{23} = 0$ , which is always an allowed solution, and minimizing the energy by varying only  $\Delta_{12}$ .) In the first case, equal pairing gaps imply that there are equal numbers of  $12$  and  $23$  pairs. Since only zero-momentum Cooper pairs are considered here, one can filter the paired atoms from the momentum distributions and determine the momentum distribution of unpaired atoms by calculating the difference  $\langle n_{\sigma k} \rangle - \langle n_{2k} \rangle / 2$  for  $\sigma = 1, 3$ . The distribution of unpaired atoms is seen to form a clear Fermi sphere, but with maximal occupation probability of 0.5. In the case of projected pairing gap in Figure 3 the pairing atoms  $|1\rangle$  and  $|2\rangle$  form a breach due to a number mismatch between the two components.

The boundary condition of fixed atom numbers for each component separately is natural for atomic gas experiments. However, the results for a homogeneous gas must be approached with caution since experiments are always conducted in nonuniform

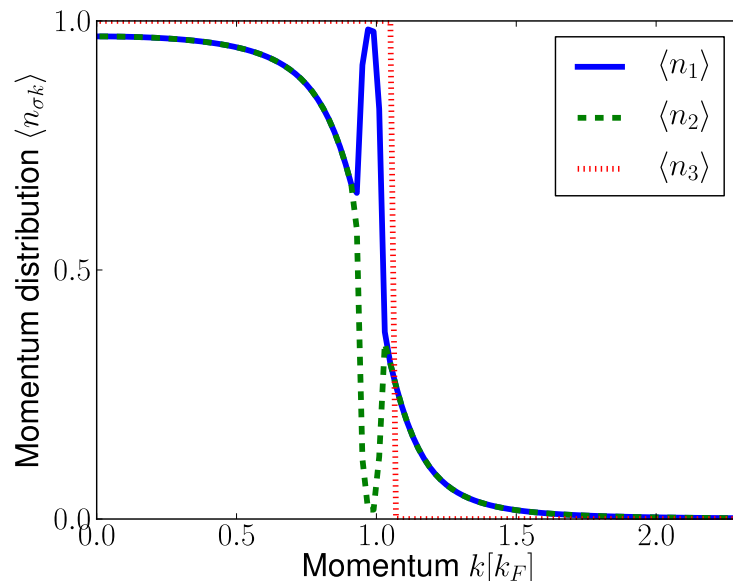


**Figure 3.** Single-particle occupation numbers as in Figure 2 but now for projected pairing field vector  $\Delta_{23} = 0, \Delta_{12} = 0.32E_F$ . All atoms in the component |3⟩ are unpaired, revealing a noninteracting Fermi sea. Due to the number mismatch between components |1⟩ and |2⟩, excess atoms in |1⟩ will form a breach.

trapping potentials. Using these homogeneous system results in conjunction with local density approximation means locally fixing the chemical potentials instead of the atom numbers. This discrepancy on which boundary condition to use can be solved by treating the trapping effects explicitly using the Bogoliubov-deGennes method.

#### 4. Harmonic trap – the Bogoliubov-deGennes method

In order to consider trapped systems, we use the Bogoliubov-deGennes method that allows the inclusion of trap effects exactly. The mean-field BdG method is not expected to be able to capture all relevant physics in the strongly interacting regime. However, in an imbalanced two-component system, it has been shown [32] that, for small polarizations and symmetric trap geometries, there is a good agreement between the mean-field BdG approach and real-space dynamical mean-field theory. We solve the three-component mean-field system in a spherically harmonic trap  $V_\sigma(\mathbf{r}) = \frac{1}{2}m_\sigma\omega_\sigma^2r^2$  using the eigenbasis of the 3-dimensional harmonic oscillator

$$\Psi_\sigma(\mathbf{r}) = \sum_{nlm} R_{\sigma n}^l(r) Y_{lm}(\Omega) c_{nlm\sigma}, \quad (5)$$

where  $Y_{lm}$  are the spherical harmonics and the radial wavefunctions are given by

$$R_{\sigma n}^l(r) = \sqrt{2}(m_\sigma\omega_\sigma)^{3/4} \sqrt{\frac{n!}{(n+l+1/2)!}} e^{-\bar{r}_\sigma^2/2} \bar{r}_\sigma^l L_n^{l+1/2}(\bar{r}_\sigma^2). \quad (6)$$

Here  $L_n^{l+1/2}(\bar{r}_\sigma^2)$  is the associated Laguerre polynomial and  $\bar{r}_\sigma \equiv r\sqrt{m_\sigma\omega_\sigma/\hbar}$ .

The mean-field Hamiltonian separates for different  $l$ -quantum numbers  $H = \sum_l H_l + C$ , such that  $[H, H_l] = 0$  and  $C$  is constant. Introducing a finite cutoff energy  $E_c$  and keeping only single-particle states with energy less than the cutoff allows writing each  $H_l$  using block matrices

$$H^l = \begin{pmatrix} \mathbf{c}_{1l}^\dagger \\ \mathbf{c}_{2l} \\ \mathbf{c}_{3l}^\dagger \end{pmatrix}^T \begin{pmatrix} \epsilon_{l1} + \mathbf{J}_{12}^l & \mathbf{F}_{12}^l & \mathbf{0} \\ \mathbf{F}_{12}^l & -\epsilon_{l2} - \mathbf{J}_2^l & \mathbf{F}_{23}^l \\ \mathbf{0} & \mathbf{F}_{23}^l & \epsilon_{l3} + \mathbf{J}_{32}^l \end{pmatrix} \begin{pmatrix} \mathbf{c}_{1l} \\ \mathbf{c}_{2l}^\dagger \\ \mathbf{c}_{3l} \end{pmatrix} \quad (7)$$

where  $\mathbf{J}_2^l = \mathbf{J}_{21}^l + \mathbf{J}_{23}^l$ . The block matrices are defined as

$$\mathbf{J}_{\sigma\sigma'}^l = \begin{pmatrix} J_{\sigma\sigma'00}^l & \cdots & J_{\sigma\sigma'0N}^l \\ \vdots & \ddots & \vdots \\ J_{\sigma\sigma'N0}^l & \cdots & J_{\sigma\sigma'NN}^l \end{pmatrix} \quad \text{and} \quad \mathbf{F}_{\sigma\sigma'}^l = \begin{pmatrix} F_{\sigma\sigma'00}^l & \cdots & F_{\sigma\sigma'0N}^l \\ \vdots & \ddots & \vdots \\ F_{\sigma\sigma'N0}^l & \cdots & F_{\sigma\sigma'NN}^l \end{pmatrix} \quad (8)$$

with the Hartree shift

$$J_{\sigma\sigma'nn'}^l = U_{\sigma\sigma'}^H \int_0^\infty dr r^2 R_{\sigma n}^l(r) n_{\sigma'}(r) R_{\sigma n'}^l(r) \quad (9)$$

and the pairing field

$$F_{\sigma\sigma'nn'}^l = \int_0^\infty dr r^2 R_{\sigma n}^l(r) \Delta_{\sigma\sigma'}(r) R_{\sigma n'}^l(r). \quad (10)$$

The connection between the interaction strength  $U_{\sigma\sigma'}^H$ , used in the Hartree shift and the bare interaction strength  $U_{\sigma\sigma'}$  will be discussed below. The energy matrix  $\epsilon_{l\sigma}$  is diagonal with elements  $\epsilon_{\sigma nl} = \hbar\omega_\sigma(2n + l + 3/2) - \mu_\sigma$  and the operator vectors are  $\mathbf{c}_{\sigma l} = [c_{\sigma 0l0} \cdots c_{\sigma N_l l0}]^T$ . We denote the number of single-particle states with fixed  $l$ , whose energy is below the cutoff, as  $N_l = [E_c/(\hbar\omega) - l - 3/2]/2$ .

Similarly to free space, the  $H_l$  matrices can be diagonalized using the Bogoliubov transformation which is provided by unitary  $3N_c^l \times 3N_c^l$ -matrices  $\mathbf{W}^l$ . By inserting the identity operator  $(\mathbf{W}^l)^\dagger \mathbf{W}^l$  between the matrix and the operator vectors, we have the quasiparticle basis as  $(\gamma_{1l} \gamma_{2l}^\dagger \gamma_{3l})^T = \mathbf{W}^l (\mathbf{c}_{1l} \mathbf{c}_{2l}^\dagger \mathbf{c}_{3l})^T$ . The rotation matrix  $\mathbf{W}^l$  is chosen such that the matrix in (7) is diagonalized.

The equations for the pairing fields and the densities are

$$\Delta_{\sigma\sigma'}(r) = \tilde{U}_{\sigma\sigma'} \sum_{nn'l} (2l+1) R_{\sigma n}^l(r) R_{\sigma n'}^l(r) \sum_j W_{\bar{\sigma} N_l + n, j}^l W_{\bar{\sigma}' N_l + n', j}^l n_F(E_j), \quad (11)$$

and

$$n_\sigma(r) = \sum_{nn'l} (2l+1) R_{\sigma n}^l(r) R_{\sigma n'}^l(r) \sum_j W_{\bar{\sigma} N_l + n, j}^l W_{\bar{\sigma} N_l + n', j}^l n_F((-1)^{\bar{\sigma}} E_j), \quad (12)$$

where  $n_F$  is the Fermi distribution and  $\bar{\sigma} = \sigma - 1$ ,  $\sigma \in \{1, 2, 3\}$ . The total number of particles in each component  $|\sigma\rangle$  is obtained by integration  $N_\sigma = \int_0^\infty dr r^2 n_\sigma(r)$ .

As in usual BCS theory, the gap equation is ultraviolet divergent, hence the energy cutoff  $E_c$ . In order to make the model cutoff independent, we follow a standard



approach [33] and use a renormalized interaction  $\tilde{U}_{\sigma\sigma'}$  but now generalized to a three-component system

$$\frac{1}{\tilde{U}_{\sigma\sigma'}(r)} = \frac{1}{U_{\sigma\sigma'}} - \frac{m_r k_{c,\sigma\sigma'}(r)}{2\hbar^2\pi^2} \alpha_{\sigma\sigma'}(r) \quad (13)$$

where

$$\alpha_{\sigma\sigma'}(r) = 1 - \frac{1}{2} \frac{k_{F,\sigma\sigma'}(r)}{k_{c,\sigma\sigma'}(r)} \ln \left( \frac{k_{c,\sigma\sigma'}(r) + k_{F,\sigma\sigma'}(r)}{k_{c,\sigma\sigma'}(r) - k_{F,\sigma\sigma'}(r)} \right). \quad (14)$$

Here the momentum cutoff  $k_{c,\sigma\sigma'}$  and local Fermi momentum  $k_{F,\sigma\sigma'}$  are defined as

$$\frac{\hbar^2 k_{c,\sigma\sigma'}^2(r)}{2m_r} = [E_c - \bar{\mu}_{\sigma\sigma'}(r)] \quad \text{and} \quad \frac{\hbar^2 k_{F,\sigma\sigma'}^2(r)}{2m_r} = [2\bar{\mu}_{\sigma\sigma'}(r) - W_\sigma(r) - W_{\sigma'}(r)], \quad (15)$$

where the local average chemical potential is

$$\bar{\mu}_{\sigma\sigma'}(r) = [\mu_\sigma - V_\sigma(r) + \mu_{\sigma'} - V_{\sigma'}(r)]/2. \quad (16)$$

We solve these gap and number equations self-consistently using fixed point iteration. For every iteration step in the gap equation, we solve the chemical potentials  $\mu_\sigma$  to keep the particle numbers constants. The iteration is terminated when the subsequent gap profiles in the iteration differ by at most  $5 \times 10^{-5} \hbar\omega$ . The cutoff energy is chosen to be  $2.5 \times \max\{E_F^\sigma\}$ , (with a higher cutoff, the results do not qualitatively change). If the convergence is slow, we try different initial values to ensure that the final result is correct. We use a small finite temperature ( $T = 10^{-3} T_F$ ) to smoothen the Fermi distribution and to help solving the number equations in presence of a discrete energy spectrum. However, we have checked that the results are unchanged even for zero temperature for example in Figures 6 and 7. We do not consider higher temperatures in this work, however, we have checked that our results are sufficiently robust to survive low but experimentally relevant temperature  $T = 0.05 T_F$ . An example of the effect of the temperature is shown in Figure 4 where exactly the same parameters as in Figure 6 are used except that  $T = 0.05 T_F$ . The results, especially the coexistence region, are practically identical, only the minor features at the edge of the gas have been smoothened.

The Hartree fields become infinite with a diverging scattering length  $a_{\sigma\sigma'} \rightarrow \infty$ . This unphysical effect is caused by improper treatment of two-body scattering effects and in practice these energy shifts are limited by the Fermi energy. Monte Carlo results on a two-component Fermi gas suggest that the Hartree fields at unitarity do not exceed  $|W| \approx 0.5 E_F$  [34, 35]. We limit the Hartree field interaction to be smaller than this value by imposing a hard cutoff on the Hartree interaction strength. That is, instead of the bare interaction  $U_{\sigma\sigma'}$  we use  $U_{\sigma\sigma'}^H$ , which is limited from above by

$$|U_{\sigma\sigma'}^H n_{\sigma'}(0)| \leq 0.5 E_F^{\sigma'}. \quad (17)$$

Notice that the component  $|2\rangle$  experiences two Hartree fields due to the two components  $|1\rangle$  and  $|3\rangle$  and thus the total Hartree shift experienced by this component can be up to double the above cutoff. Since the Hartree shifts induce a mismatch between the Fermi surfaces, the pairing amplitude is reduced. Notice that this is in contrast

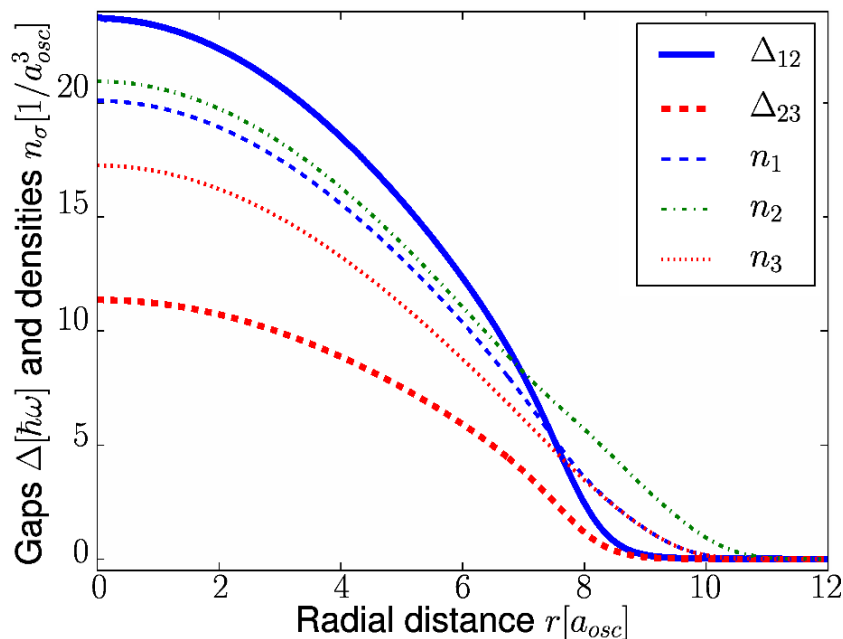


**Figure 4.** Typical gap and density profiles in harmonic trap calculated for temperature  $T = 0.05 T_F$ . Other parameters are the same as in Figure 6.

to the balanced two-component case in which both components experience the same Hartree potential and the densities remain thus equal. In three component systems, the inclusion of the third interaction  $U_{13}$  would reduce the mismatch, but because it is usually weaker, the mismatch does not totally disappear. However, the mismatch can be countered by careful choice of interaction strengths and atom numbers, so that local density imbalances are reduced.

The Hartree shift can be seen to produce interesting shell structures for certain parameters. Such exotic shell structures created by the Hartree shift will be considered elsewhere, requiring a more complete treatment of the Hartree effect to confirm their validity. In the present work, we have chosen to focus on a parameter range in which these peculiar features are not present and in all of the results shown in this work except in Figure 5 we neglect the Hartree effects, i.e. we use  $U_{\sigma\sigma'}^H = 0$  for all  $\sigma, \sigma'$ . Our choice does not significantly limit the parameter range, because these effects appeared always only in tiny islands in the parameter space, typically at the edges of the trap. Indeed, we have checked that the inclusion of the Hartree shift in the way described above does not qualitatively change the results presented here. An example is shown in Figure 5, which presents the case of Figure 6 but with Hartree fields included. The qualitative behaviour is the same although the numerical values of the order parameters are smaller. Importantly, the Hartree fields do not affect the coexistence of the two order parameters.

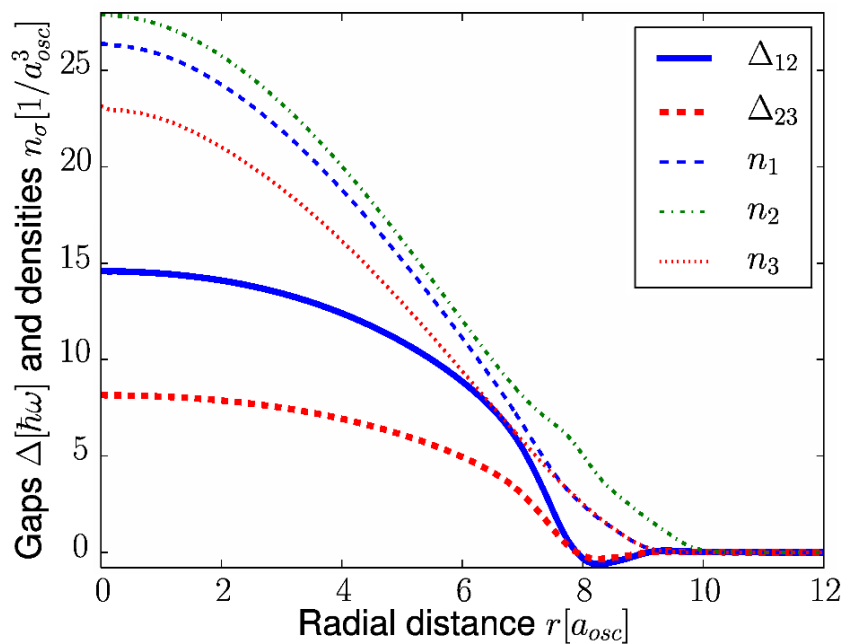


**Figure 5.** Typical gap and density profiles in harmonic trap calculated for zero temperature but including the Hartree energy shift in the way described in the main text. The parameters are the same as in Figure 6.

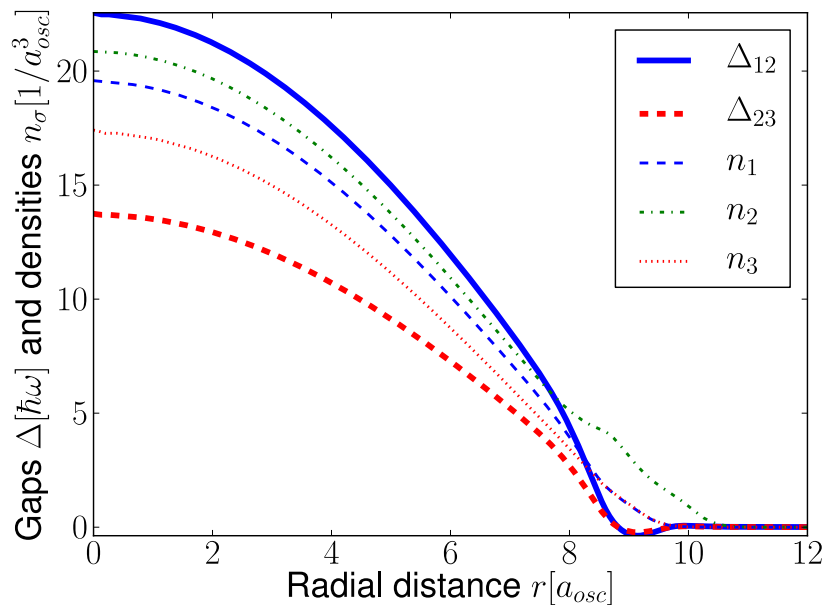


**Figure 6.** Typical gap and density profiles in harmonic trap showing a large coexistence region of the pairing fields  $\Delta_{12}$  and  $\Delta_{23}$ . The parameters are  $N_2 = 3 \times 10^4$ ,  $N_1 = 0.8N_2$ ,  $N_3 = 0.7N_2$ , and  $(k_F a_{12})^{-1} = (k_F a_{23})^{-1} = -0.50$ .

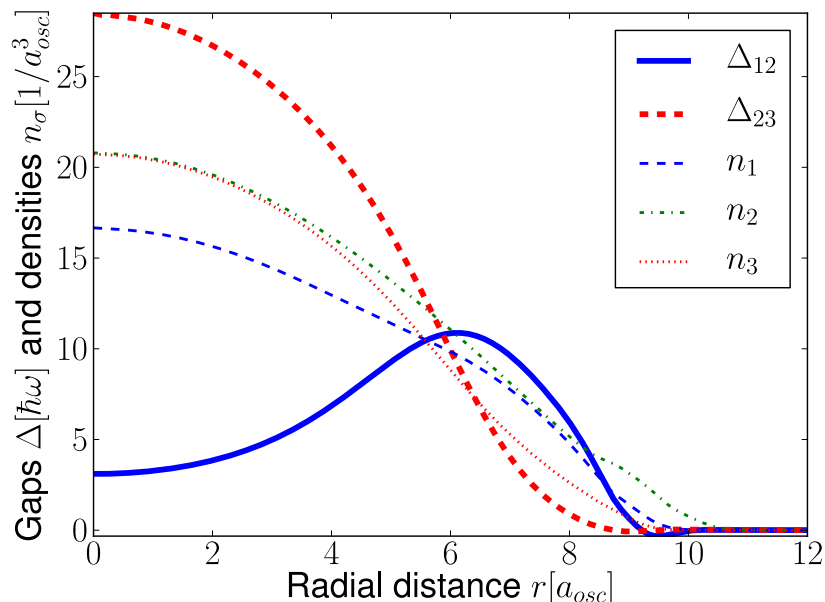


**Figure 7.** Gap and density profiles as in Figure 6 but for mismatched interaction strengths  $(k_F a_{12})^{-1} = -0.50$ ,  $(k_F a_{23})^{-1} = -0.45$ . The two pairing fields  $\Delta_{12}$  and  $\Delta_{23}$  separate into different regions, with a  $\Delta_{23}$  core surrounded by a  $\Delta_{12}$  shell.

## 5. Results

Figures 6 and 7 show typical gap and density profiles obtained from the BdG method. In the former the gaps follow the density distributions, and the two pairing gaps  $\Delta_{12}$  and  $\Delta_{23}$  are present across the trap. In the latter the gaps are spatially separated, with the  $\Delta_{12}$  pairing field concentrated at the edge of the trap and  $\Delta_{23}$  at the center of the trap. There is no clear interface between the two pairing regions, but the penetration length of pairing field  $\Delta_{12}$  inside  $\Delta_{23}$  is relatively constant when increasing the system size (increasing atom numbers  $N$ ), characteristic length scale given by the oscillator length  $r_{\text{osc}} = \sqrt{\hbar/m_2\omega_2}$ . Locally the dominating pairing channel is the one for which the atom densities are least mismatched, the strength of the interaction being only a secondary factor. This local nature of pairing allows interesting shell structures [36] as shown in Figure 7. However, we do not pursue these issues here but rather concentrate on more general features. Notice that the number of atoms in component  $|3\rangle$  has been chosen to be slightly smaller than in components  $|1\rangle$  and  $|2\rangle$ , but the features shown here are very general.

Figures 8 a) and b) show the pairing fields  $\Delta_{12}$  and  $\Delta_{23}$  as a function of interaction strength  $(k_F a_{23})^{-1}$ . When either of the two interaction strengths  $a_{12}$ ,  $a_{23}$  is significantly stronger, the corresponding pairing channel will dominate. The crossover between the two regions occurs at  $(k_F a_{23})^{-1} = -0.46$  (not at  $(k_F a_{23})^{-1} = -0.50$  because of the atom number mismatch  $N_1 > N_3$ ). To better characterize the coexistence of the two pairing

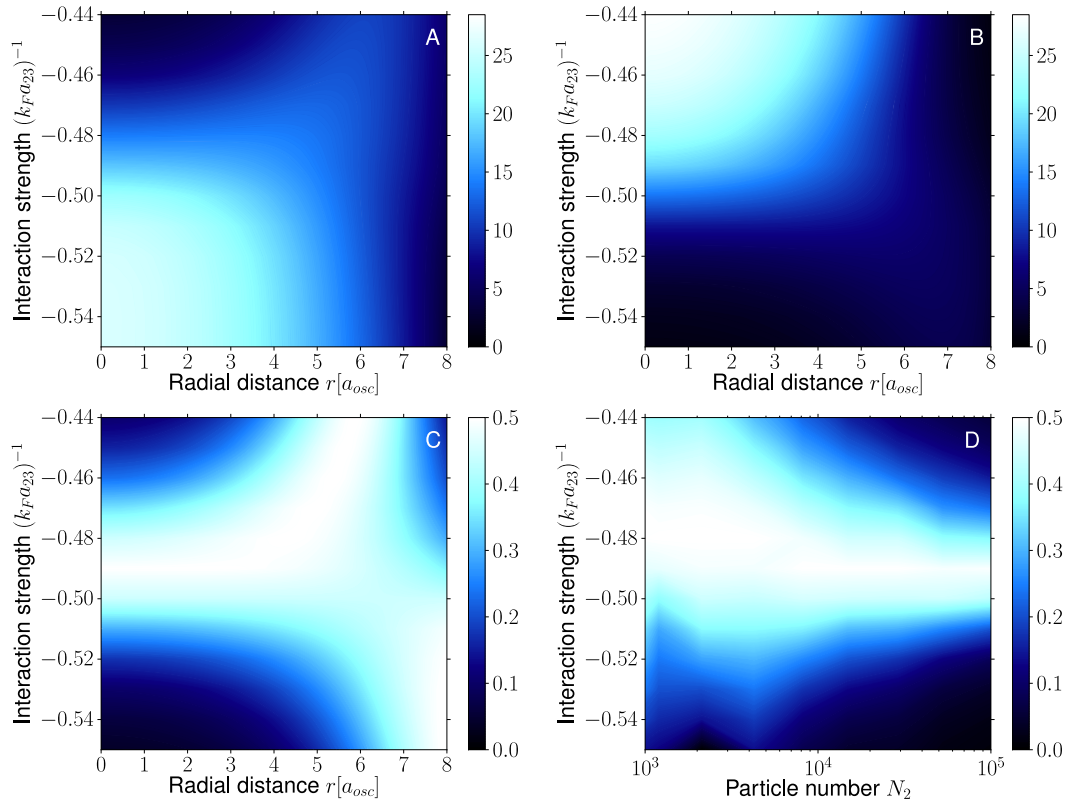


**Figure 8.** (a) Pairing field  $\Delta_{12}$  (in units of  $\hbar\omega$ ) as a function of the interaction strength  $U_{23}$ . (b) Pairing field  $\Delta_{23}$ . (c) The coexistence parameter  $P_{co} = \Delta_{12}\Delta_{23}/(\Delta_{12}^2 + \Delta_{23}^2)$  shows the coexistence areas. Atom numbers in a), b) and c) are the same as in Figure 6. In (d) the coexistence parameter is plotted at  $r = 0$  for different numbers of particles  $N$ .

gaps, we define a dimensionless *coexistence* parameter

$$P_{co} = \frac{\Delta_{12}\Delta_{23}}{\Delta_{12}^2 + \Delta_{23}^2}. \quad (18)$$

Figure 8 c) shows this parameter as a function of interaction strength and position, revealing a large coexistence region in the somewhat narrow interaction strength window  $-0.51 < (k_F a_{23})^{-1} < -0.47$ , but also a coexistence region close to the edge of the trap across a wide range of interactions. In Figure 8 d) we show how the coexistence parameter at the center of the trap scales with increasing system size  $N$  (the atom numbers  $N_1$  and  $N_3$  are scaled correspondingly so that the relative polarizations are fixed). The coexistence area is suppressed as  $N$  grows large, implying that the coexistence may vanish in the thermodynamic  $N \rightarrow \infty$  limit. However, with sufficiently accurate choice of interaction strengths, the coexistence region should be experimentally accessible with reasonably sized atom gases. We have not studied the scaling of the coexistence regions at the edge of the trap, but since the penetration length in Figure 7 is given by the oscillator length we expect the  $N \rightarrow \infty$  limit to yield a phase separation into a  $\Delta_{23}$  core and a surrounding  $\Delta_{12}$  shell.

To better understand the nature of the pairing scheme in the coexistence areas,

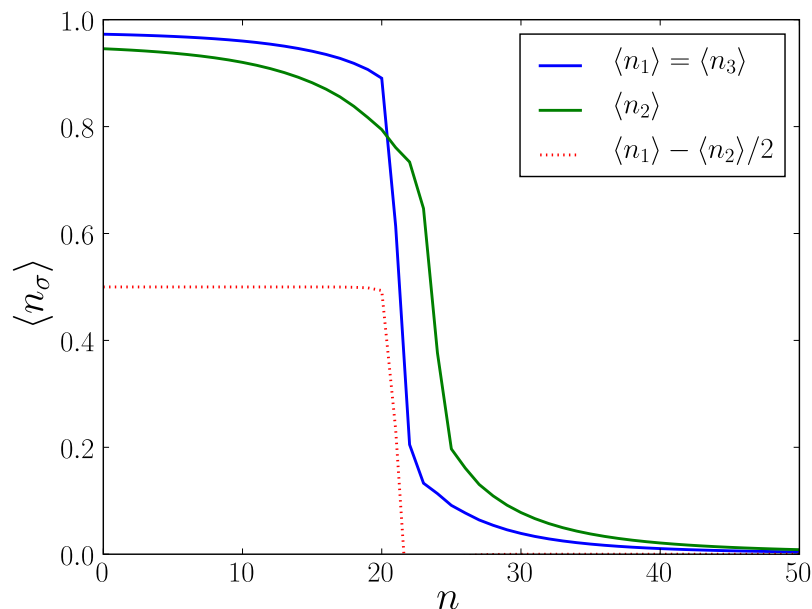


**Figure 9.** Occupation numbers  $\langle n_{\sigma n, l=0} \rangle = \langle c_{\sigma n 0}^\dagger c_{\sigma n 0} \rangle$  for each component  $\sigma$  as a function of the quantum number  $n$  with  $l = 0$ . The parameters have been chosen symmetrically  $N_1 = N_3 = 16000$ ,  $N_2 = 20000$ , and  $(k_F a_{12})^{-1} = (k_F a_{23})^{-1} = -0.50$ , resulting in identical pairing gaps  $\Delta_{12}(r) = \Delta_{23}(r)$ .

Figure 9 a) shows the occupation numbers of different  $n$ -quantum number states for a symmetric case  $\Delta_{12}(r) \equiv \Delta_{13}(r)$ . The angular momentum quantum number  $l = 0$  chosen here acts as a representative of a more general behavior for general  $l$ . The figure reveals a very similar pairing scheme as in the homogeneous system, see Figure 2. The unpaired atoms are distributed among the two components  $|1\rangle$  and  $|3\rangle$  and form a step at the Fermi surface.

## 6. Conclusions

We have studied the pairing of a three-component Fermi gas when two of the interspecies interaction channels are dominant. In a homogeneous system, we showed that different boundary conditions, namely fixing the chemical potential or fixing the atom numbers, produce qualitatively different results and phases. We have not considered the possibility of a phase separation in which the two pairing fields would be spatially separated in otherwise uniform system.

For trapped systems, our BdG study reveals an interesting coexistence region where both pairing channels  $\Delta_{12}$  and  $\Delta_{23}$  are present. This is a mesoscopic effect and likely to vanish in the limit of a large system  $N \rightarrow \infty$  resulting in phase separation into shells of different pairing fields. However, the coexistence region is present at atom numbers relevant for atom gas experiments, making the observation of this intriguing double-gap prediction feasible.

There is already a wide range of standard experimental techniques to detect such

pairing correlations. For example, one could use radio-frequency spectroscopy [37, 38, 39] for driving atoms from the hyperfine states  $|1\rangle$  and  $|3\rangle$  separately into some fourth noninteracting state  $|e\rangle$ . Other possibilities include transforming pairing correlations into molecular 12 and/or 23 pairs through magnetic field sweeps [40] or optical molecular spectroscopy [41].

## Acknowledgements

We acknowledge funding from Academy of Finland and EUROQUAM/FerMix (Project No. 210953, No. 213362, No. 217045, No. 217043). This work was conducted as a part of a EURYI scheme grant, see [www.esf.org/euryi](http://www.esf.org/euryi).

## References

- [1] P. Fulde and R. A. Ferrell. Superconductivity in a strong spin-exchange field. *Phys. Rev.*, 135(3A):A550, 1964.
- [2] A.I. Larkin and Yu.N. Ovchinnikov. Nonuniform state of superconductors. *Sov Phys JETP*, 20:762, 1965.
- [3] W. Vincent Liu and F. Wilczek. Interior gap superfluidity. *Phys. Rev. Lett.*, 90(4):047002, 2003.
- [4] T. B. Ottenstein, T. Lompe, M. Kohnen, A. N. Wenz, and S. Jochim. Collisional stability of a three-component degenerate Fermi gas. *Phys. Rev. Lett.*, 101(20):203202, 2008.
- [5] J. H. Huckans, J. R. Williams, E. L. Hazlett, R. W. Stites, and K. M. O’Hara. Three-body recombination in a three-state Fermi gas with widely tunable interactions. *Phys. Rev. Lett.*, 102(16):165302, 2009.
- [6] J. R. Williams, E. L. Hazlett, J. H. Huckans, R. W. Stites, Y. Zhang, and K. M. O’Hara. Evidence for an excited-state Efimov trimer in a three-component Fermi gas. *Phys. Rev. Lett.*, 103(13):130404, 2009.
- [7] A. N. Wenz, T. Lompe, T. B. Ottenstein, F. Serwane, G. Zürn, and S. Jochim. Universal trimer in a three-component Fermi gas. *Phys. Rev. A*, 80(4):040702, 2009.
- [8] T. Lompe, T. B. Ottenstein, F. Serwane, K. Viering, A. N. Wenz, G. Zürn, and S. Jochim. Atom-dimer scattering in a three-component Fermi gas. *Phys. Rev. Lett.*, 105(10):103201, 2010.
- [9] Á. Rapp, G. Zaránd, C. Honerkamp, and W. Hofstetter. Color superfluidity and “baryon” formation in ultracold fermions. *Phys. Rev. Lett.*, 98(16):160405, 2007.
- [10] S. Capponi, G. Roux, P. Lecheminant, P. Azaria, E. Boulat, and S. R. White. Molecular superfluid phase in systems of one-dimensional multicomponent fermionic cold atoms. *Phys. Rev. A*, 77(1):013624, 2008.
- [11] K. Inaba and S.I. Suga. Finite-temperature properties of attractive three-component fermionic atoms in optical lattices. *Phys. Rev. A*, 80(4):041602, 2009.
- [12] P. Azaria, S. Capponi, and P. Lecheminant. Three-component Fermi gas in a one-dimensional optical lattice. *Phys. Rev. A*, 80(4):041604, 2009.
- [13] A. Kantian, M. Dalmonte, S. Diehl, W. Hofstetter, P. Zoller, and A. J. Daley. Atomic color superfluid via three-body loss. *Phys. Rev. Lett.*, 103(24):240401, 2009.
- [14] G. Klingschat and C. Honerkamp. Exact diagonalization study of trionic crossover and trion liquid in the attractive three-component Hubbard model. *Phys. Rev. B*, 82(9):094521, 2010.
- [15] A. Luscher and A. Laeuchli. Imbalanced three-component Fermi gas with attractive interactions: Multiple FFLO-pairing, Bose-Fermi and Fermi-Fermi mixtures versus collapse and phase separation. *arXiv:0906.0768*, 2009.
- [16] A.G.W. Modawi and A.J. Leggett. Some properties of a spin-1 Fermi superfluid: Application to spin-polarized  ${}^6\text{Li}$ . *J. Low Temp. Phys.*, 109:625–39, 1997.

- [17] C. Honerkamp and W. Hofstetter. Ultracold fermions and the  $SU(N)$  Hubbard model. *Phys. Rev. Lett.*, 92(17):170403, 2004.
- [18] C. Honerkamp and W. Hofstetter. BCS pairing in Fermi systems with  $N$  different hyperfine states. *Phys. Rev. B*, 70(9):094521, 2004.
- [19] T. Paananen, J.-P. Martikainen, and P. Törmä. Pairing in a three-component Fermi gas. *Phys. Rev. A*, 73(5):053606, 2006.
- [20] L. He, M. Jin, and P. Zhuang. Superfluidity in a three-flavor Fermi gas with  $SU(3)$  symmetry. *Phys. Rev. A*, 74(3):033604, 2006.
- [21] R. W. Cherng, G. Refael, and E. Demler. Superfluidity and magnetism in multicomponent ultracold fermions. *Phys. Rev. Lett.*, 99(13):130406, 2007.
- [22] G. Catelani and E. A. Yuzbashyan. Phase diagram, extended domain walls, and soft collective modes in a three-component fermionic superfluid. *Phys. Rev. A*, 78(3):033615, 2008.
- [23] P. F. Bedaque and J. P. D’Incao. Superfluid phases of the three-species fermion gas. *Annals of Physics*, 324(8):1763, 2009.
- [24] S. Chiacchiera, T. Macrì, and A. Trombettoni. Dipole oscillations in fermionic mixtures. *Phys. Rev. A*, 81(3):033624, 2010.
- [25] T. Ozawa and G. Baym. Population imbalance and pairing in the BCS-BEC crossover of three-component ultracold fermions. *Phys. Rev. A*, 82(6):063615, 2010.
- [26] M. K. Tey, S. Stellmer, R. Grimm, and F. Schreck. Double-degenerate Bose-Fermi mixture of strontium. *Phys. Rev. A*, 82(1):011608, 2010.
- [27] M. Bartenstein, A. Altmeyer, S. Riedl, R. Geursen, S. Jochim, C. Chin, J. Hecker Denschlag, R. Grimm, A. Simoni, E. Tiesinga, C. J. Williams, and P. S. Julienne. Precise determination of  $\text{Li}^6$  cold collision parameters by radio-frequency spectroscopy on weakly bound molecules. *Phys. Rev. Lett.*, 94(10):103201, 2005.
- [28] C. A. Regal, M. Greiner, and D. S. Jin. Lifetime of molecule-atom mixtures near a Feshbach resonance in  $\text{K}^{40}$ . *Phys. Rev. Lett.*, 92(8):083201, 2004.
- [29] F. M. Spiegelhalter, A. Trenkwalder, D. Naik, G. Hendl, F. Schreck, and R. Grimm. Collisional stability of  $^{40}\text{K}$  immersed in a strongly interacting Fermi gas of  $^6\text{Li}$ . *Phys. Rev. Lett.*, 103(22):223203, 2009.
- [30] F. M. Spiegelhalter, A. Trenkwalder, D. Naik, G. Kerner, E. Wille, G. Hendl, F. Schreck, and R. Grimm. All-optical production of a degenerate mixture of  $^6\text{Li}$  and  $^{40}\text{K}$  and creation of heteronuclear molecules. *Phys. Rev. A*, 81(4):043637, 2010.
- [31] J.-P. Martikainen, J. J. Kinnunen, P. Törmä, and C. J. Pethick. Induced interactions and the superfluid transition temperature in a three-component Fermi gas. *Phys. Rev. Lett.*, 103(26):260403, 2009.
- [32] D.-H. Kim, J. J. Kinnunen, J.-P. Martikainen, and P. Törmä. Exotic superfluid states of lattice fermions in elongated traps. *Phys. Rev. Lett.*, 106(9):095301, 2011.
- [33] M. Grasso and M. Urban. Hartree-Fock-Bogoliubov theory versus local-density approximation for superfluid trapped fermionic atoms. *Phys. Rev. A*, 68(3):033610, 2003.
- [34] P. Magierski, G. Wlazłowski, A. Bulgac, and J. E. Drut. Finite-temperature pairing gap of a unitary Fermi gas by quantum monte carlo calculations. *Phys. Rev. Lett.*, 103(21):210403, 2009.
- [35] R. Haussmann, M. Punk, and W. Zwerger. Spectral functions and rf response of ultracold fermionic atoms. *Phys. Rev. A*, 80(6):063612, 2009.
- [36] T. Paananen, P. Törmä, and J. P. Martikainen. Co-existence and shell structures of several superfluids in trapped three-component Fermi mixtures. *Phys. Rev. A*, 75:023622, 2007.
- [37] P. Törmä and P. Zoller. Laser probing of Cooper pairs. *Phys. Rev. Lett.*, 85:487, 2000.
- [38] C. Chin, M. Bartenstein, A. Altmeyer, S. Riedl, S. Jochim, J. H. Denschlag, and R. Grimm. Observation of the pairing gap in a strongly interacting Fermi gas. *Science*, 305:1128–1130, 2004.
- [39] J. Kinnunen, M. Rodriguez, and P. Törmä. Pairing gap and in-gap excitations in trapped fermionic



- superfluids. *Science*, 305:1131–1133, 2004.
- [40] C. A. Regal, M. Greiner, and D. S. Jin. Observation of resonance condensation of fermionic atom pairs. *Phys. Rev. Lett.*, 92(4):040403, 2004.
- [41] G. B. Partridge, K. E. Strecker, R. I. Kamar, M. W. Jack, and R. G. Hulet. Molecular probe of pairing in the BEC-BCS crossover. *Phys. Rev. Lett.*, 95(2):020404, 2005.